HHS Public Access

Author manuscript

J Biomech. Author manuscript; available in PMC 2018 July 26.

Published in final edited form as:

J Biomech. 2017 July 26; 60: 134–141. doi:10.1016/j.jbiomech.2017.06.031.

Biomechanical properties of murine TMJ articular disc and condyle cartilage via AFM-nanoindentation

Prashant Chandrasekaran[a,1], **Basak Doyran**[a,1], **Qing Li**[a], **Biao Han**[a], **Till E. Bechtold**[b,c], **Eiki Koyama**[b], **X. Lucas Lu**[d], and **Lin Han**[a,*]

[a]School of Biomedical Engineering, Science, and Health Systems, Drexel University, Philadelphia, PA 19104, United States

[b]Department of Surgery, The Children's Hospital of Philadelphia, Philadelphia, PA 19104, United States

[c]Department of Orthodontics, University Hospital, University of Tübingen, Tübingen 72076, Germany

[d]Department of Mechanical Engineering, University of Delaware, Newark, DE 19716, United States

Abstract

This study aims to quantify the biomechanical properties of murine temporomandibular joint (TMJ) articular disc and condyle cartilage using AFM-nanoindentation. For skeletally mature, 3-month old mice, the surface of condyle cartilage was found to be significantly stiffer (306 ± 84 kPa, mean ± 95% CI) than those of the superior (85 ± 23 kPa) and inferior (45 ± 12 kPa) sides of the articular disc. On the disc surface, significant heterogeneity was also detected across multiple anatomical sites, with the posterior end being the stiffest and central region being the softest. Using SEM, this study also found that the surfaces of disc are composed of anteroposteriorly oriented collagen fibers, which are sporadically covered by thinner random fibrils. Such fibrous nature results in both an $F\text{-}D^{3/2}$ indentation response, which is a typical Hertzian response for soft continuum tissue under a spherical tip, and a linear $F\text{-}D$ response, which is typical for fibrous tissues, further signifying the high degree of tissue heterogeneity. In comparison, the surface of condyle cartilage is dominated by thinner, randomly oriented collagen fibrils, leading to Hertzian-dominated indentation responses. As the first biomechanical study of murine TMJ, this work will provide a basis for future investigations of TMJ tissue development and osteoarthritis in various murine TMJ models.

Keywords

Temporomandibular joint; Murine models; Fibrocartilage; Nanoindentation; Heterogeneity

Corresponding author. Fax: +1 215 895 4983. lh535@drexel.edu.

[1]These author s contributed equally to this work.

Conflict of interest statement

The authors of this study have no personal or financial conflicts of interest with this work. All authors were fully involved in the study and preparation of this manuscript and the material within has not been and will not be submitted for publication elsewhere.

1. Introduction

In the temporomandibular joint (TMJ), the articular disc and mandibular condyle cartilage play key biomechanical roles in daily activities such as chewing and speaking (Tanaka and Koolstra, 2008). The TMJ disc is a fibrocartilage mainly composed of anteroposteriorly aligned type I collagen fibers with minute amount of proteoglycans (Detamore and Athanasiou, 2003). The mandibular condyle cartilage is a hybrid of fibro- and hyaline cartilage, in which, a surface fibrocartilage layer with anteroposterior type I collagen fibers covers a secondary layer of proteoglycan-rich hyaline cartilage (Singh and Detamore, 2008) (Fig. 1a). Such structural features endow these tissues with specialized nonlinear, anisotropic and heterogeneous biomechanical properties crucial to TMJ function. These properties include several orders higher tensile modulus compared to the compressive modulus (Allen and Athanasiou, 2006; Singh and Detamore, 2009a), the higher tensile (Detamore and Athanasiou, 2003; Singh and Detamore, 2008) and shear (Tanaka et al., 2003; Tanaka et al., 2008b) moduli along the anteroposterior orientation than those along the mediolateral orientation, as well as lower surface friction coefficient along the anteroposterior orientation (Ruggiero et al., 2015).

TMJ osteoarthritis (TMJ OA), the most prevalent degenerative TMJ disease (Das, 2013), has been reported to affect 10–30% of the population (Rando and Waldron, 2012), and can be present even without clinical symptoms (Bertram et al., 2001). In TMJ OA, both the disc and condyle cartilage undergo irreversible degradation, leading to abnormal joint contact, craniomandibular pain and limited jaw motion (Wang et al., 2015). In seeking for effective treatment and functional repair strategies, murine model becomes a necessary and unique in vivo platform, as its availability for genetic modification and short lifespan enable pinpointing the TMJ development, biology and pathogenesis to specific molecules or signaling pathways (Suzuki and Iwata, 2016). Evaluation of the phenotype in genetically modified mice has provided new insights into the roles of individual matrix molecules in TMJ development and OA, such as lubricin (Bechtold et al., 2016; Hill et al., 2014; Koyama et al., 2014), biglycan and fibromodulin (Wadhwa et al., 2005), collagen types II (Ricks et al., 2013) and XI (Xu et al., 2003). In addition, aided by clinically relevant operations such as partial discectomy (Xu et al., 2009) and anterior crossbite prosthesis (Liu et al., 2014), TMJ OA can be induced in mice to study the disease initiation and progression in a well-defined timeframe in vivo.

In these studies, developmental phenotype and disease symptoms of the TMJ were mainly evaluated by biochemical and histological assays. While these tools clearly illustrated the compositional and tissue-level structural changes, they did not elucidate changes in the biomechanical functions of TMJ during development or disease. The mechanical knowledge, however, is critical, for that the primary function of the TMJ is biomechanical. In addition, as mechanical properties are integrated responses of tissue extracellular matrix (ECM) composition and structure (Hung and Ateshian, 2016), they could be more sensitive to disease-induced degradation than biochemical or structural parameters. Currently, limited by the small size of the murine TMJ tissues, conventional macroscopic biomechanical tests are not applicable. Without such understanding, biological activities observed in murine

models cannot be directly connected with the TMJ function or disease-associated dysfunction.

The objective of this study is to define the collagen fibril structure and biomechanical properties of murine TMJ disc and condylar cartilage (Fig. 1a). To this end, nanoindentation fits well with the scope, given its capability of mechanical testing at the micro-scale, which is demonstrated by several studies applying atomic force microscopy (AFM) (Hu et al., 2001; Patel and Mao, 2003) and instrumented (Yuya et al., 2010) nanoindentation on larger animal TMJs. Using AFM-nanoindentation, we quantified the mechanical properties of TMJ disc and condyle cartilage in skeletally mature, wild-type mice, including indentation modulus, loading rate effects, and location-dependent heterogeneity. The micromechanical properties were analyzed in the context of collagen fibril nanostructure of both the disc and condyle cartilage surfaces. We expect that the new biomechanical understanding of healthy murine TMJ tissues can serve as a benchmark for future investigations of TMJ development, aging and disease-associated mechanical changes in various transgenic or induced TMJ OA murine models.

2. Methods

2.1. Sample preparation

TMJ condyle heads and articular discs were harvested from skeletally mature, 3-month-old C57BL/6 mice (The Jackson Laboratory) and glued onto AFM discs by a cyanoacrylate adhesive gel (Loctite 409, Henkel Corp., Rocky Hill, CT). The condyle head and disc were excised out of the murine TMJ by exposing the mandibular region and cleaning the cheek muscle. Care was taken to remove these tissues by isolating the condyle head and the disc, and then separating them. Once the separation was achieved, tissues were rinsed thoroughly by PBS (pH = 7.4) with protease inhibitors (Pierce, Thermo Fisher, Rockford, IL). After rinsing, these tissues were cleaned under a microscope carefully by keeping the forceps away from the surface of each tissue. The debris and other soft tissues surrounding the white periphery of the disc were cleaned without damaging the interior of the ring, by individually removing each with utmost care. Samples were then preserved in PBS (pH = 7.4) with protease inhibitors at 4 °C for less than 24 h before the mechanical test. No statistical differences were observed in the mechanical properties of left versus right discs or condyle cartilage tissues. Therefore, for each mouse, condyle cartilage from either the left or the right TMJ was tested. To study both superior and inferior surfaces of the disc, we tested one disc on the superior (tubercle) side, and the other one from the same mouse on the inferior (condyle) side (Fig. 1b).

2.2. AFM-nanoindentation

Microspherical AFM tips were prepared by end-attaching borosilicate colloids ($R \approx 5$ μm) onto the end of a tipless cantilever (nominal $k \approx 2$ N/m, NSC36-B, NanoAndMore, Lady's Island, SC) using the M-Bond 610 epoxy (Polysciences), following our established procedure (Li et al., 2015). This process was performed by using the optical microscope and z-step motor of the Dimension Icon AFM (Bruker-Nano, Santa Barbara, CA) as the micro-manipulator. After the attachment, the tip was cured at room temperature in ambient

conditions for a minimum of 48 h to stabilize the attachment. AFM-nanoindentation was then performed on the surfaces of TMJ condyle cartilage and disc using the microspherical tip and a Dimension Icon AFM in PBS with protease inhibitors to maintain the physiological-like fluidic environment. For condyle cartilage ($n = 10$), since access to the non-central regions is limited by its irregular shape, nanoindentation was only performed on the central region. Benefited from the flat geometry of the disc, nanoindentation was performed on five anatomical regions: anterior, posterior, central, medial and lateral regions on both the superior (tubercle) and inferior (condyle) sides ($n = 7$ on each side). For each tissue and region, indentation was carried out up to ≈ 150 nN maximum force at 1–10 μm/s rates for at least 10 different locations within each region.

The effective indentation modulus, E_{ind}, was calculated by fitting the whole loading portion of force-indentation depth, *F-D*, curve to the Hertz model with finite thickness correction

$$F=\frac{4}{3}\frac{E_{\mathrm{ind}}}{(1-\nu^2)}R^{1/2}D^{3/2}C_{\chi}(R,D,H,\nu) \quad (1)$$

where R is the tip radius, ν is the Poisson's ratio (≈0 for both condyle cartilage (Hagandora et al., 2011) and TMJ disc (Kim et al., 2003)) and C_{χ} is the substrate constraint correction factor that depends on R, D, H, and ν (Dimitriadis et al., 2002). For the articular disc, the tissue thickness, H, is measured via histological pictures, where $H = 30.3 \pm 8.0$ μm (mean ± 95% CI over 20 measurements on 3 animals) in the center region and $H > 100$ μm in the other regions (113 ± 23 μm at the posterior, 117 ± 24 μm at the anterior of the disc, 115 ± 2 μm at the medial and lateral ends). Thickness of the condyle cartilage, including both the fibrous and hyaline layers, is also >100 μm.

2.3. Structural analysis

After nanoindentation, TMJ condyle cartilage and both sides of articular discs were exposed to enzymatic digestion to enable direct visualization of the collagen fibrils on the surface. First, tissues were incubated in 0.1 mg/mL bovine pancreatic trypsin (Sigma-Aldrich, St. Louis, MO) in PBS (pH = 7.4) at 37 °C for 24 h to remove the proteoglycans, as previously described (Rojas et al., 2014). Second, samples were then incubated in 0.4 U/mL hyaluronidase (Sigma-Aldrich, St. Louise, MO) in PBS with 10 mM sodium acetate (pH = 6.0) at 37 °C for 24 h to remove the proteoglycans and expose the collagen fibril architecture. Afterwards, samples were fixed with Karnovsky's fixative (Electron Microscopy Sciences, Hatfield, PA), dehydrated in a series of graded de-ionized water-ethanol and ethanol-hexamethyldisilazane (HMDS) mixtures (Bray et al., 1993), and dried in air to retain the 3D collagen architecture. SEM (Zeiss Supra 50VP) images were acquired on samples coated with ~6 nm thick platinum. From each image, the diameter of each collagen fibril was measured via ImageJ. For histology, additional mice were euthanized, and the entire inferior TMJ joint, including condyle and TMJ disc, were harvested, fixed in 4% paraformaldehyde, decalcified in 10% EDTA and embedded in paraffin. Sagittal sections were cut across the joint and stained with Safranin-O/Fast Green and Hema-toxylin&Eosin (H&E) to reveal the whole joint morphology (Fig. 1a).

2.4. Statistical analysis

Non-parametric statistical tests were used to avoid the assumption of normal distribution. To evaluate the regional heterogeneity across all five regions on each side of the articular disc, two-way analysis of the variance (ANOVA) on the global rank transformation followed by Tukey-Kramer post hoc multiple comparison was performed on the mechanical moduli at all different regions and different animals. The anatomical region was taken as a fixed effect, and the animal number was taken as a randomized effect. To study the micromechanical heterogeneity within each individual disc, Kruskal-Wallis test followed by Tukey-Kramer multiple comparison was performed through all locations measured on five regions of each disc surface. To examine the significance of loading rate dependence, Friedman's test was performed on all locations measured at 1 – 10 μm/s rates within each region of interest on the disc and condyle surfaces. For fibril diameter analysis, as ≥300 fibrils (from n = 3 animals) were measured on each surface, according to the central limit theorem, the parametric one-way ANOVA followed by Tukey-Kramer multiple comparison was performed to compare the diameters across the three tissue surfaces.

3. Results

The mandibular condyle had the significantly higher modulus E_{ind} (306 ± 84 kPa, mean ± 95% CI) than the TMJ disc (superior surface, 81 ± 23 kPa; inferior surface 45 ± 12 kPa) (n ≥7 via Mann-Whitney U test, Fig. 2a). Under AFM-nanoindentation, with a maximum indenting depth < 1.5 μm, the outcomes mainly reflect the top ~10 to 15 μm layer of tissue surface (~10 × indenting depth). For TMJ disc, since the thickness is ~30 μm in the thinnest central region, E_{ind} here reflects the apparent loading behaviors of the bulk tissue. However, for the condyle cartilage, as the fibrocartilage layer is >100 μm thick, E_{ind} represents only the properties of the top fibrocartilage layer, not the secondary hyaline cartilage layer (Fig. 1a). On the surfaces of TMJ disc, E_{ind} was found to vary significantly with anatomical regions, with highest modulus at the posterior end, lowest at the center, and similar moduli amongst other sites (Fig. 2b). This trend was consistent on both the superior and inferior sides. Within each individual animal, significant heterogeneity in E_{ind} was also observed, and was similar to the overall trend shown in Fig. 2b (shown for one representative animal in Fig. 3a, Kruskal-Wallis test followed by Tukey-Kramer multiple comparison). Meanwhile, significant loading rate-dependence in E_{ind} was observed on all three tissues. As shown for measurements of each surface on one animal, varying indentation depth rate for one order (1–10 μm/s) results in 33 ± 10%, 54 ± 10% and 76 ± 33% increase in E_{ind} for the condyle, superior and inferior surfaces of the disc, respectively (Fig. 3b).

SEM images revealed detailed collagen fibril structure on the surfaces of mandibular condyle cartilage and articular disc. The condyle cartilage surface was dominated by randomly oriented collagen fibrils (Fig. 4), which is similar to the surface of articular hyaline cartilage of murine knee joints (Batista et al., 2014). In contrast, on the articular disc surface, two types of collagen fibrils can be observed. A majority of the fibrils were highly aligned and aggregated to form fibers (Fig. 5). These fibers are aligned along or near the anteroposterior orientation, similar to the observations on larger animal TMJ disc and condyle cartilage (Shengyi and Xu, 1991). On both superior and inferior surfaces, there also

exist randomly oriented, thinner fibrils. The estimated fibril diameters were 22.3 ± 0.3 nm (mean ± 95% CI from ≥300 fibrils measured on $n = 3$ animals) for the condyle cartilage surface, which were significantly thinner ($p < 0.0001$) than those on the disc surfaces (33.4 ± 0.4 for superior surface, 32.9 ± 0.5 for inferior surface, both of which are statistically similar) (Fig. 6a). In addition, variations of fibril diameters were also noted on the disc surfaces. On the superior side, the anterior end appeared to have the thickest fibrils (35.6 ± 1.1 nm), and the medial region had the thinnest (31.3 ± 0.8 nm); on the inferior side, the anterior end also had the thickest fibrils (34.0 ± 1.0 nm), and the central region had the thinnest (31.2 ± 0.9 nm) (Fig. 6b).

4. Discussion

4.1. Specialized biomechanical properties of murine TMJ tissues

This study elucidates the specialized micromechanical characteristics of murine TMJ disc and condyle cartilage. Notably, the condyle cartilage surface has ≈5–8 times higher modulus than that of the disc (Fig. 2a). This difference can be likely attributed to differences in collagen fibril structure and cross-linking on TMJ condyle surface than those on disc surfaces. When fibrous tissues are deformed by spherical indenters, the *F-D* curves represent an integrated response of both compressive and tensile resistance of collagen fibrils. The surface of condyle cartilage is dominated by random fibrils, while both sides of disc surfaces have more aligned fibers with larger diameters (Figs. 4, 5). While the higher degree of alignment and larger diameters on disc surfaces (Fig. 6) may indicate higher modulus, the SEM imaging on condyle surface is likely not to represent the bulk structure of the fibrous layer. It is possible that the interior of condyle cartilage has a higher degree of cross-link density, and possibly thicker fibrils underneath the surface layer, similar to other fibrocartilage tissues such as the meniscus (Li et al., 2017; Petersen and Tillmann, 1998). These characteristics can contribute to the observed higher modulus on the condyle cartilage.

This modulus contrast between the disc and condyle cartilage is distinct from the TMJs of larger animals. Under unconfined compression, the adult porcine TMJ exhibits region-dependent equilibrium modulus of ~20 to 170 kPa for the disc (Allen and Athanasiou, 2006) and ~10 to 22 kPa for the condyle cartilage (Singh and Detamore, 2009b). Similarly, for adult hircine TMJ under unconfined compression, the axial modulus is ~20 kPa for the disc and ~10 kPa for the condyle cartilage at low strains (~10%) (Hagandora et al., 2011). Under tension, the adult porcine disc is stiffer than condyle cartilage along the anteroposterior orientation, where in the central region, the relaxed tensile modulus is 18.5 ± 4.9 MPa for the disc (mean ± std), and 8.8 ± 4.1 MPa for the condyle cartilage (Detamore and Athanasiou, 2003; Singh and Detamore, 2008). This trend is reversed along the mediolateral orientation, where in the intermediate region, the relaxed modulus is 0.58 ± 0.39 MPa for the disc, and 3.6 ± 2.0 MPa for the condyle cartilage (Detamore and Athanasiou, 2003; Singh and Detamore, 2008). While these uniaxial test results do not show that the TMJ discs of larger animals have substantially lower resistance to indentation than the condyle cartilage, under spherical microindentation ($R \approx 0.8$ mm), porcine condyle cartilage is shown to have substantially higher aggregated modulus than the disc when tested at similar forces, with 36

± 9 kPa for the disc and 250 ± 60 kPa for the condyle cartilage (mean ± std) (Lu et al., 2009; Zimmerman et al., 2015). These quantitative results thus suggest that the >5 × higher modulus observed on murine condyle cartilage (Fig. 2) could possibly indicate a response specific to the multiaxial loading executed by the spherical indentation. Meanwhile, as highlighted by the thickness contrast between murine TMJ disc and condyle cartilage, which is absent in human TMJ (Bibb et al., 1993; Wright et al., 2016) (Fig. 7), it also possibly reflects a feature specific to the anatomy and loading of rodent TMJs, which is distinct from those of larger species including human.

In murine TMJ, the thickness of disc (≈30 μm in the central region) is much less than that of condyle cartilage (the fibro- and hyaline cartilage layers together >100 μm), while in larger animals, these two tissues have comparable thicknesses (Fig. 7, schematics are adapted from and inspired by (Suzuki and Iwata, 2016)). During the articulation of TMJ, through direct load transmission with the condyle, the disc provides a cushion effect to facilitate dissipating energy and to prevent direct condyle-temporal fossa contact that impacts brain (Chin et al., 1996). In the TMJ of larger animal, this cushion effect can arise from the intrinsic energy dissipative, poroviscoelastic deformation of the mm-thick disc. However, in murine TMJ, despite the presence of salient rate dependent mechanics (Fig. 3a), this effect is likely less important due to the small volume, μm-scale thickness of the disc (e.g., Figs. 1a, 7)). The lower modulus enables greater deformation of the murine disc during joint movement, which effectively improves the disc-contact congruency, enlarges the loading area, and reduces the contact stress on condyle and temporal fossa. The more compliant disc thus provides an extra cushion effect to reduce the impact on skull during the jaw movement. In the mean time, other structural and biomechanical factors could also contribute to the differences between murine and human TMJs, such as the diet habit (soft versus hard food and size of food) (Liu et al., 1998), anatomy of the jaw (Fig. 7) (Suzuki and Iwata, 2016), range of jaw motion during speaking and eating (Byrd, 1988), as well as the resulting loading patterns to the TMJ (Sobue et al., 2011). A more comprehensive understanding of the contrast between murine versus human TMJ structure and biomechanics can provide a basis for the use of murine models in understanding human TMJ development and disease pathogenesis.

4.2. Micromechanical heterogeneity of TMJ disc

For the TMJ disc, the asymmetry of modulus on superior versus inferior surfaces (Figs. 2b, 3a) is also likely to be associated with the unique morphology of murine TMJ. Since the disc is in direct contact with the condyle through its inferior side, a larger deformation on this side is beneficial for disc-condyle congruency, while the higher stiffness of the superior side can facilitate sustaining tensile stresses, and re-distributing tensile loads to the temporal bone (Tanaka et al., 2008a). On both surfaces, the thinnest central regions have the lowest modulus, which, at the same time, also undergoes the highest disc-condyle contact stress. The reduced modulus therefore can assist larger deformation at the center to enhance disc-condyle congruency and reduce point contact stress. The posterior ends on both sides have higher moduli than other regions. This can be associated with the fact that the tensile and shear stress is primarily along the anteroposterior orientation (Beatty et al., 2001), and the posterior end possibly sustains higher stress than other regions. This regional heterogeneity is also different from the disc of larger animal discs, in which, while the posterior and

anterior ends are stiffer, the central region has similar moduli as the medial and lateral ends (Willard et al., 2012).

4.3. Collagen nanostructure-mechanics relationships

In accordance with the presence of anteroposterior fibril alignment on disc surfaces, indentation *F-D* curves show two different behaviors. One group yields the typical $F\text{-}D^{3/2}$ Hertzian dependence (type I in Fig. 8, 72 ± 6% on superior surface, 86 ± 4% on inferior surface, mean ± 95% CI), while the other group yields a non-Hertzian, close to linear *F-D* behavior (type II in Fig. 8, 28 ± 6% on superior surface, 14 ± 4% on inferior surface), signified by higher coefficient of determination R^2 from the linear fit. For soft tissues, indentation by spherical tips normally produces nonlinear increase in force versus depth, for that the tip-contact area increases in a near hyperbolic manner with indentation depth (Lin et al., 2009). The elastic Hertz contact model, which predicts a $F\text{-}D^{3/2}$ dependence for the contact between a rigid sphere and a planar continuum material (e.g., Eq. (1)), can sufficiently describe the indentation responses in the regime where material stress-strain response is linear (strain $\varepsilon < 20\%$, and $D < 0.4R$ (Lin et al., 2009)). Here, the non-Hertzian, close to linear *F-D* response is possible when the indentation is performed on the highly aligned, larger collagen fibers. In this case, loading vertical to the fiber axis mainly induces tensile stretch of fibers. This linear *F-D* response has also been shown in other fibrous tissues whose surface are dominated by highly aligned collagen fibrils, such as murine meniscus (Li et al., 2015) and chicken embryonic tendon (Marturano et al., 2013). In comparison, this linear response is absent on condyle cartilage surface, which consists of transversely random fibrils (Fig. 4). The disc surface collagen structure also likely contributes to the boundary lubrication of the disc, in which, the friction coefficient along the anteroposterior orientation, i.e., the collagen fiber axis, is lower than that along the mediolateral orientation (Ruggiero et al., 2015).

4.4. Limitation and future work

Restricted by the shape of the mandibular condyle, we were not able to assess all five regions of the condyle surface. The >100 μm thickness of the superficial fibrocartilage layer also prevented us to quantify the properties of the secondary hyaline cartilage layer. In addition, while this study clearly shows the presence of rate-dependence, we did not aim to elucidate the exact deformation mechanisms. Since the surfaces of both disc and condyle cartilage are fibrocartilage tissues with minute proteoglycans, this rate-dependent mechanics is likely a combination of intrinsic viscoelasticity due to intra- and inter-fibril interactions as well as fluid flow induced poroelasticity, which can be distinctive from the aggrecan-rich hyaline cartilage. Our ongoing studies aim to address these limitations, and to provide a comprehensive understanding of the murine TMJ biomechanics.

5. Conclusions

This study is the first to define the nanostructural and micromechanical properties of the articular disc and mandibular cartilage of the murine TMJ articular disc and mandibular condyle cartilage, as well as the condyle-disc contact mechanics and micromechanical heterogeneity of the disc. The observed non-Hertzian indentation response signifies the

fibrous nature of TMJ disc. Given the differences observed in the biomechanical properties of murine and human TMJs, these features underscore the unique biomechanics of murine TMJs. With the knowledge learned from healthy, wild-type murine TMJ, our results, in combination with more advanced AFM micromechanical techniques, will enable a more thorough evaluation of the function-relevant biomechanical properties of healthy TMJs and those undergoing pathological degenerative conditions in murine models.

Acknowledgments

This work was supported by the National Institutes of Health (NIH) Grants AR066824 to LH, DE023841 to EK, and AR050950 to the Penn Center for Musculoskeletal Disorders (PCMD), as well as the Osteo Science Foundation Research Award to XLL.

References

Allen KD, Athanasiou KA. Viscoelastic characterization of the porcine temporomandibular joint disc under unconfined compression. J Biomech. 2006; 39:312–322. [PubMed: 16321633]

Batista MA, Nia HT, Önnerfjord P, Cox KA, Ortiz C, Grodzinsky AJ, Heinegård D, Han L. Nanomechanical phenotype of chondroadherin-null murine articular cartilage. Matrix Biol. 2014; 38:84–90. [PubMed: 24892719]

Beatty MW, Bruno MJ, Iwasaki LR, Nickel JC. Strain rate dependent orthotropic properties of pristine and impulsively loaded porcine temporomandibular joint disk. J Biomed Mater Res. 2001; 57:25–34. [PubMed: 11416845]

Bechtold TE, Saunders C, Mundy C, Um H, Decker RS, Salhab I, Kurio N, Billings PC, Pacifici M, Nah HD, Koyama E. Excess BMP signaling in heterotopic cartilage forming in *Prg4*-null TMJ discs. J Dent Res. 2016; 95:292–301. [PubMed: 26534931]

Bertram S, Rudisch A, Innerhofer K, Pumpel E, Grubwieser G, Emshoff R. Diagnosing TMJ internal derangement and osteoarthritis with magnetic resonance imaging. J Am Dent Assoc. 2001; 132:753–761. [PubMed: 11433854]

Bibb CA, Pullinger AG, Baldioceda F. Serial variation in histological character of articular soft tissue in young human adult temporomandibular joint condyles. Arch Oral Biol. 1993; 38:343–352. [PubMed: 8517806]

Bray DF, Bagu J, Koegler P. Comparison of hexamethyldisilazane (HMDS), peldri II, and critical-point drying methods for scanning electron-microscopy of biological specimens. Microsc Res Tech. 1993; 26:489–495. [PubMed: 8305726]

Byrd KE. Opto-electronic analyses of masticatory mandibular movements and velocities in the rat. Arch Oral Biol. 1988; 33:209–215. [PubMed: 3178540]

Chin LP, Aker FD, Zarrinnia K. The viscoelastic properties of the human temporomandibular joint disc. J Oral Maxillofac Surg. 1996; 54:315–318. discussion 318–319. [PubMed: 8600239]

Das SK. TMJ osteoarthritis and early diagnosis. J Oral Biol Craniofac Res. 2013; 3:109–110. [PubMed: 25737896]

Detamore MS, Athanasiou KA. Tensile properties of the porcine temporomandibular joint disc. J Biomech Eng. 2003; 125:558–565. [PubMed: 12968581]

Dimitriadis EK, Horkay F, Maresca J, Kachar B, Chadwick RS. Determination of elastic moduli of thin layers of soft material using the atomic force microscope. Biophys J. 2002; 82:2798–2810. [PubMed: 11964265]

Hagandora CK, Chase TW, Almarza AJ. A comparison of the mechanical properties of the goat temporomandibular joint disc to the mandibular condylar cartilage in unconfined compression. J Dent Biomech. 2011; 2011:212385. [PubMed: 21765875]

Hill A, Duran J, Purcell P. Lubricin protects the temporomandibular joint surfaces from degeneration. PLoS ONE. 2014; 9:e106497. [PubMed: 25188282]

Hu K, Radhakrishnan P, Patel RV, Mao JJ. Regional structural and viscoelastic properties of fibrocartilage upon dynamic nanoindentation of the articular condyle. J Struct Biol. 2001; 136:46–52. [PubMed: 11858706]

Hung CT, Ateshian GA. Grading of osteoarthritic cartilage: correlations between histology and biomechanics. J Orthop Res. 2016; 34:8–9. [PubMed: 26694218]

Kim KW, Wong ME, Helfrick JF, Thomas JB, Athanasiou KA. Biomechanical tissue characterization of the superior joint space of the porcine temporomandibular joint. Ann Biomed Eng. 2003; 31:924–930. [PubMed: 12918907]

Koyama E, Saunders C, Salhab I, Decker RS, Chen I, Um H, Pacifici M, Nah HD. Lubricin is required for the structural integrity and post-natal maintenance of TMJ. J Dent Res. 2014; 93:663–670. [PubMed: 24834922]

Li Q, Doyran B, Gamer LW, Lu XL, Qin L, Ortiz C, Grodzinsky AJ, Rosen V, Han L. Biomechanical properties of murine meniscus surface via AFM-based nanoindentation. J Biomech. 2015; 48:1364–1370. [PubMed: 25817332]

Li Q, Qu F, Han B, Wang C, Li H, Mauck RL, Han L. Micromechanical anisotropy and heterogeneity of the meniscus extracellular matrix. Acta Biomater. 2017; 54:356–366. [PubMed: 28242455]

Lin DC, Shreiber DI, Dimitriadis EK, Horkay F. Spherical indentation of soft matter beyond the Hertzian regime: numerical and experimental validation of hyperelastic models. Biomech Model Mechanobiol. 2009; 8:345–358. [PubMed: 18979205]

Liu ZJ, Ikeda K, Harada S, Kasahara Y, Ito G. Functional properties of jaw and tongue muscles in rats fed a liquid diet after being weaned. J Dent Res. 1998; 77:366–376. [PubMed: 9465169]

Liu YD, Liao LF, Zhang HY, Lu L, Jiao K, Zhang M, Zhang J, He JJ, Wu YP, Chen D, Wang MQ. Reducing dietary loading decreases mouse temporomandibular joint degradation induced by anterior crossbite prosthesis. Osteoarthr Cartilage. 2014; 22:302–312.

Lu XL, Mow VC, Guo XE. Proteoglycans and mechanical behavior of condylar cartilage. J Dent Res. 2009; 88:244–248. [PubMed: 19329458]

Marturano JE, Arena JD, Schiller ZA, Georgakoudi I, Kuo CK. Characterization of mechanical and biochemical properties of developing embryonic tendon. Proc Natl Acad Sci U S A. 2013; 110:6370–6375. [PubMed: 23576745]

Patel RV, Mao JJ. Microstructural and elastic properties of the extracellular matrices of the superficial zone of neonatal articular cartilage by atomic force microscopy. Front Biosci. 2003; 8:A18–A25. [PubMed: 12456328]

Petersen W, Tillmann B. Collagenous fibril texture of the human knee joint menisci. Anat Embryol. 1998; 197:317–324. [PubMed: 9565324]

Rando C, Waldron T. TMJ osteoarthritis: a new approach to diagnosis. Am J Phys Anthropol. 2012; 148:45–53. [PubMed: 22371124]

Ricks ML, Farrell JT, Falk DJ, Holt DW, Rees M, Carr J, Williams T, Nichols BA, Bridgewater LC, Reynolds PR, Kooyman DL, Seegmiller RE. Osteoarthritis in temporomandibular joint of Col2a1 mutant mice. Arch Oral Biol. 2013; 58:1092–1099. [PubMed: 23518238]

Rojas FP, Batista MA, Lindburg CA, Dean D, Grodzinsky AJ, Ortiz C, Han L. Molecular adhesion between cartilage extracellular matrix macromolecules. Biomacromolecules. 2014; 15:772–780. [PubMed: 24491174]

Ruggiero L, Zimmerman BK, Park M, Han L, Wang L, Burris DL, Lu XL. Roles of the fibrous superficial zone in the mechanical behavior of TMJ condylar cartilage. Ann Biomed Eng. 2015; 43:2652–2662. [PubMed: 25893511]

Shengyi T, Xu Y. Biomechanical properties and collagen fiber orientation of TMJ discs in dogs: Part 1. Gross anatomy and collagen fiber orientation of the discs. J Craniomandib Disord. 1991; 5:28–34. [PubMed: 1809767]

Singh M, Detamore MS. Tensile properties of the mandibular condylar cartilage. J Biomech Eng. 2008; 130:011009. [PubMed: 18298185]

Singh M, Detamore MS. Biomechanical properties of the mandibular condylar cartilage and their relevance to the TMJ disc. J Biomech. 2009a; 42:405–417. [PubMed: 19200995]

Singh M, Detamore MS. Stress relaxation behavior of mandibular condylar cartilage under high-strain compression. J Biomech Eng. 2009b; 131:061008. [PubMed: 19449962]

Sobue T, Yeh WC, Chhibber A, Utreja A, Diaz-Doran V, Adams D, Kalajzic Z, Chen J, Wadhwa S. Murine TMJ loading causes increased proliferation and chondrocyte maturation. J Dent Res. 2011; 90:512–516. [PubMed: 21248355]

Suzuki A, Iwata J. Mouse genetic models for temporomandibular joint development and disorders. Oral Dis. 2016; 22:33–38. [PubMed: 26096083]

Tanaka E, Koolstra JH. Biomechanics of the temporomandibular joint. J Dent Res. 2008; 87:989–991. [PubMed: 18946004]

Tanaka E, Hanaoka K, van Eijden T, Tanaka M, Watanabe M, Nishi M, Kawai N, Murata H, Hamada T, Tanne K. Dynamic shear properties of the temporomandibular joint disc. J Dent Res. 2003; 82:228–231. [PubMed: 12598554]

Tanaka E, Detamore MS, Tanimoto K, Kawai N. Lubrication of the temporomandibular joint. Ann Biomed Eng. 2008a; 36:14–29. [PubMed: 17985243]

Tanaka E, Iwabuchi Y, Rego EB, Koolstra JH, Yamano E, Hasegawa T, Kawazoe A, Kawai N, Tanne K. Dynamic shear behavior of mandibular condylar cartilage is dependent on testing direction. J Biomech. 2008b; 41:1119–1123. [PubMed: 18242620]

Wadhwa S, Embree M, Ameye L, Young MF. Mice deficient in biglycan and fibromodulin as a model for temporomandibular joint osteoarthritis. Cells Tissues Organs. 2005; 181:136–143. [PubMed: 16612079]

Wang XD, Zhang JN, Gan YH, Zhou YH. Current understanding of pathogenesis and treatment of TMJ osteoarthritis. J Dent Res. 2015; 94:666–673. [PubMed: 25744069]

Willard VP, Kalpakci KN, Reimer AJ, Athanasiou KA. The regional contribution of glycosaminoglycans to temporomandibular joint disc compressive properties. J Biomech Eng. 2012; 134:011011. [PubMed: 22482666]

Wright GJ, Coombs MC, Hepfer RG, Damon BJ, Bacro TH, Lecholop MK, Slate EH, Yao H. Tensile biomechanical properties of human temporomandibular joint disc: effects of direction, region and sex. J Biomech. 2016; 49:3762–3769. [PubMed: 27743627]

Xu L, Flahiff CM, Waldman BA, Wu D, Olsen BR, Setton LA, Li Y. Osteoarthritis-like changes and decreased mechanical function of articular cartilage in the joints of mice with the chondrodysplasia gene (cho). Arthritis Rheum. 2003; 48:2509–2518. [PubMed: 13130470]

Xu L, Polur I, Lim C, Servais JM, Dobeck J, Li Y, Olsen BR. Early-onset osteoarthritis of mouse temporomandibular joint induced by partial discectomy. Osteoarthr Cartilage. 2009; 17:917–922.

Yuya PA, Amborn EK, Beatty MW, Turner JA. Evaluating anisotropic properties in the porcine temporomandibular joint disc using nanoindentation. Ann Biomed Eng. 2010; 38:2428–2437. [PubMed: 20195763]

Zimmerman BK, Bonnevie ED, Park M, Zhou Y, Wang L, Burris DL, Lu XL. Role of interstitial fluid pressurization in TMJ lubrication. J Dent Res. 2015; 94:85–92. [PubMed: 25297115]

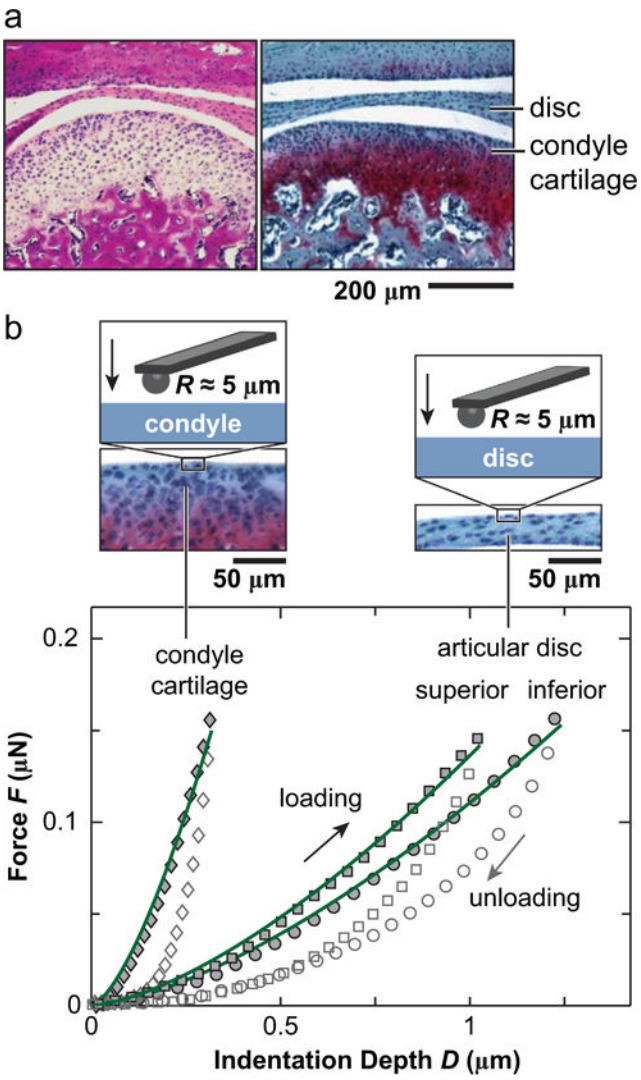

Fig. 1.

(a) Hematoxylin & Eosin (left) and Safranin-O/Fast Green (right) histology of sagittal sections showed the morphology of murine TMJ, highlighting the tissues of interest in this study: articular disc and mandibular condyle cartilage. (b) Representative indentation force versus depth, *F-D*, curves measured on the central regions of articular disc and mandibular condyle surfaces at 10 μm/s rate. The symbols are experimental data (density reduced for clarity), and solid lines are associated Hertz model fits to each of the loading *F-D* curve.

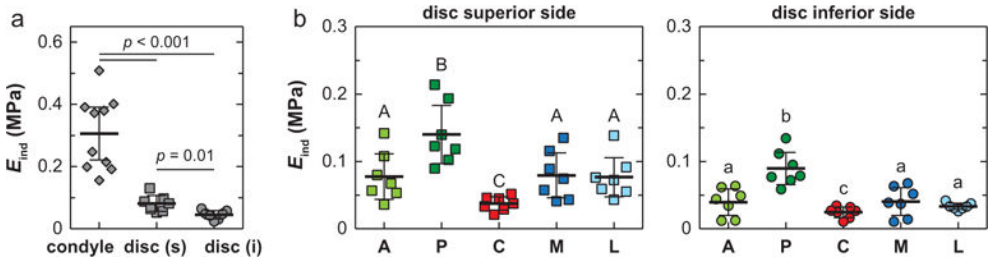

Fig. 2.

Effective indentation modulus, E_{ind}, of 3-month old murine TMJ articular disc and condyle cartilage surfaces ($n = 7$ for each side of disc, and $n = 10$ for condyle cartilage, measured at 10 μm/s rate). (a) Comparison across three tissue sites. For condyle cartilage, each data point represents averaged values of ≥10 locations measured on the central region of one animal. For articular disc, each data point represents averaged value of ≥40 locations measured on all five regions of each animal. (b) Comparison across five different anatomical regions on the articular disc surface (A: anterior, P: posterior, C: central, M: medial, L: lateral), each data point represents averaged value of ≥8 locations measured on each region of one animal. Regions with different letters are statistically different ($p < 0.05$, mean ± 95% CI).

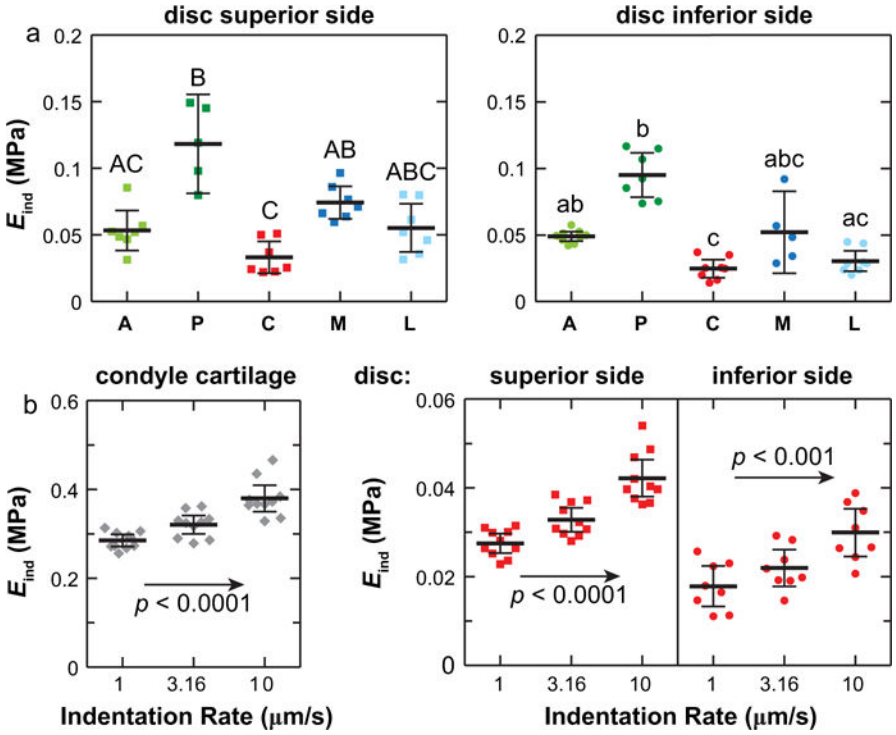

Fig. 3.

Heterogeneity and rate-dependence of E_{ind} within individual animal. (a) Variation of E_{ind} on the superior and inferior surfaces of TMJ articular disc from one mouse measured at 10 μm/s rate. (b) Rate-dependence of E_{ind} measured on the central regions of TMJ condyle cartilage and articular disc from one mouse. Each data point represents one indentation location (≥8 locations measured on each region of one animal, $p < 0.05$, mean ± 95% CI).

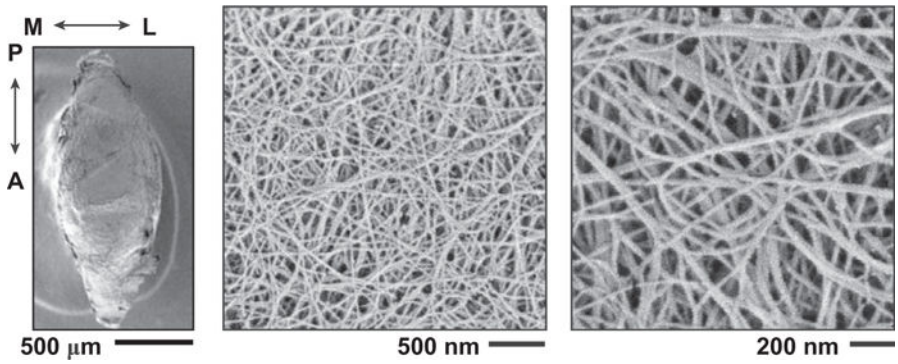

Fig. 4.

SEM images of the central region of the mandibular condyle cartilage surface. The other four regions have similar fibrillar structure, and thus, are not shown.

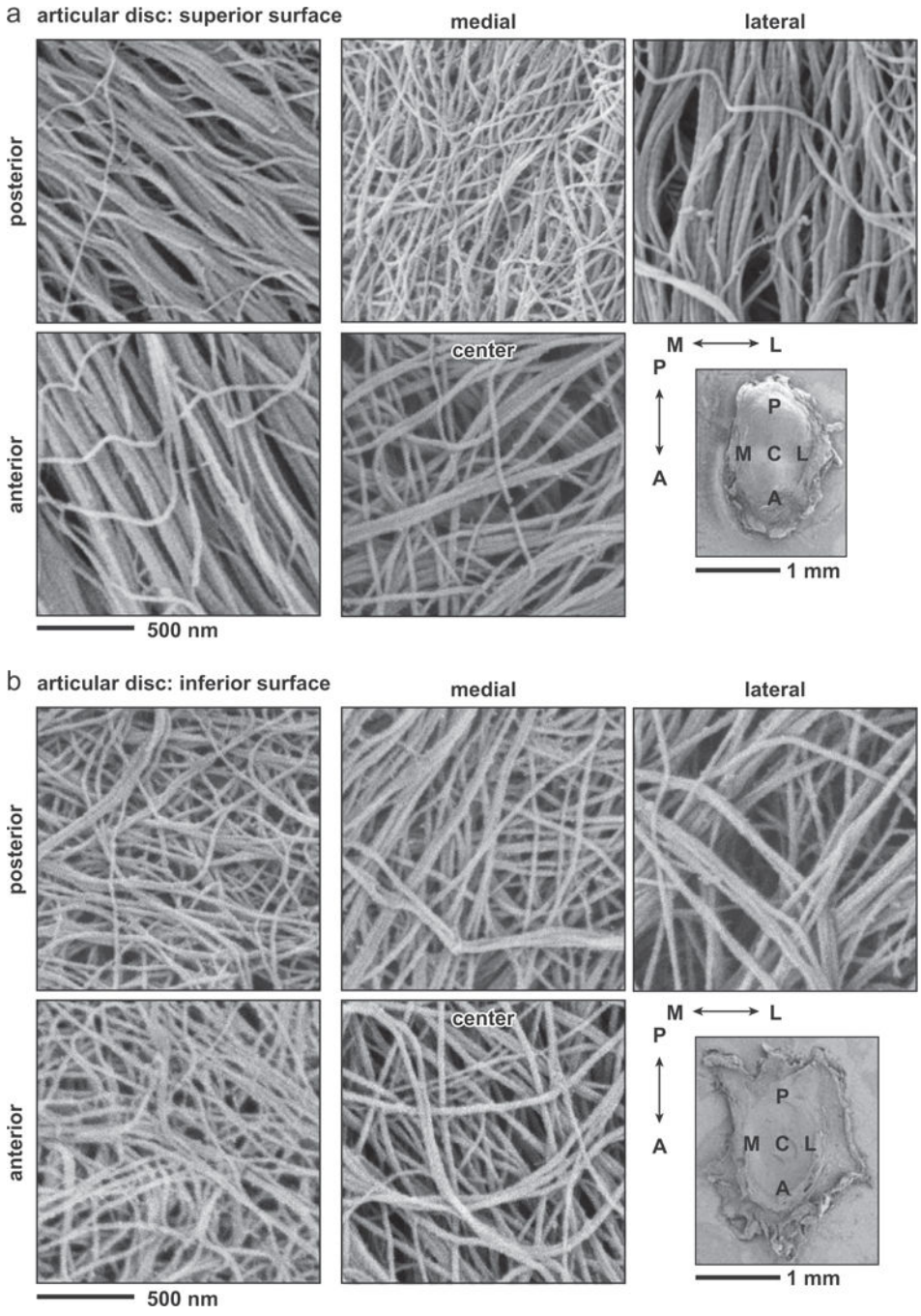

Fig. 5.

SEM images of five different anatomical regions on (a) superior and (b) inferior sides of the articular disc surface.

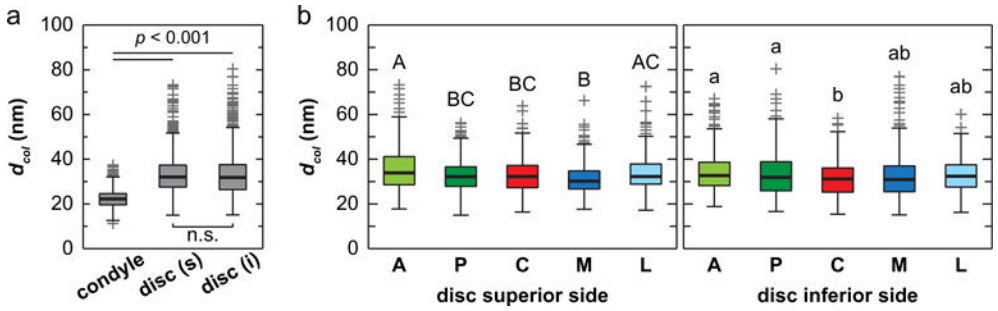

Fig. 6.

Distribution of collagen fibril diameters measured on the surfaces of TMJ articular disc and mandibular condyle cartilage. (a) Comparison across the three tissue sites (for each disc surface, measurements were pooled from all five different regions), (b) Comparison across five different anatomical regions on the articular disc surface (A: anterior, P: posterior, C: central, M: medial, L: lateral) (≥300 fibrils from $n = 3$ animals for each region, regions with different letters are statistically different, $p < 0.05$, mean ± 95% CI).

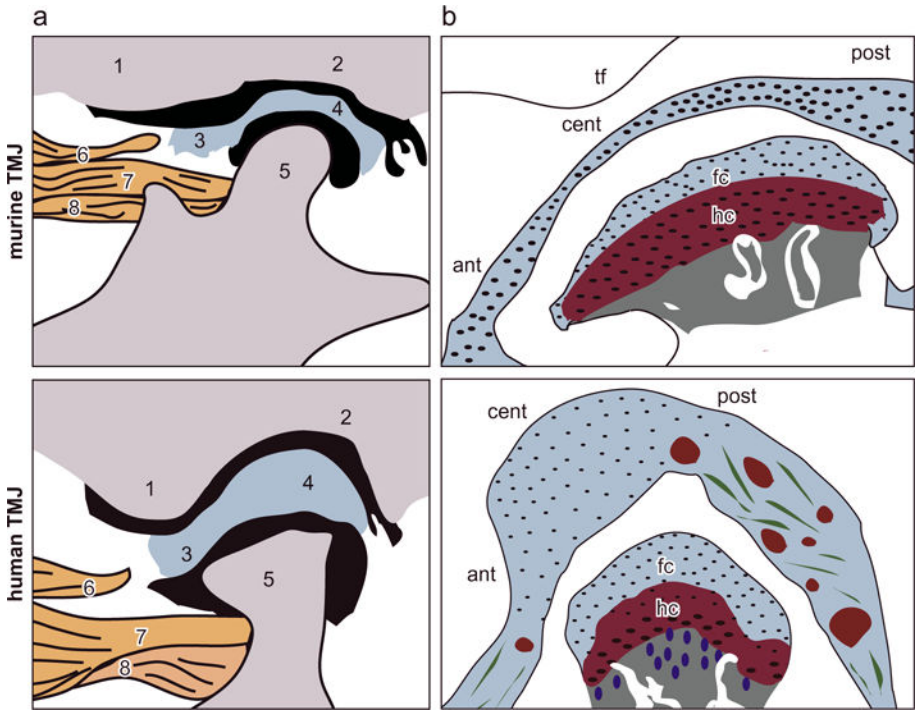

Fig. 7.

Schematics of the anatomical structure of murine versus human TMJs. (a) Anatomical structure of the TMJ: 1. articular eminence of temporal bone, 2. glenoid fossa of temporal bone, 3. anterior band of the articular disc, 4. posterior band of the articular disc, 5. mandibular condyle, 6. upper head of lateral pterygoid muscle, 7. upper head of the lateral pterygoid muscle connected to the mandible and 8. lower head of the lateral pterygoid muscle connected to the mandible condyle (adapted from (Suzuki and Iwata (2016)) with permission). (b) More detailed schematics of TMJ disc and condyle cartilage structure. In the murine TMJ, the articular disc has substantially smaller thickness compared to the condyle cartilage. This contrast is absent in larger animal TMJs (abbreviations, tf: temporal fossa, ant: anterior end, cent: central region, post: posterior end, fc: fibrocartilage, hc: hyaline cartilage). The tissue thickness values are: human: TMJ disc ~0.5–3 mm, condyle fibrocartilage layer: 400–600 μm, hyaline cartilage layer ~300–600 μm, as estimated in Bibb et al. (1993), Wright et al. (2016); murine TMJ disc ~30–60 μm, condyle fibrocartilage layer ~25–40 μm, hyaline cartilage layer ~90–120 μm.

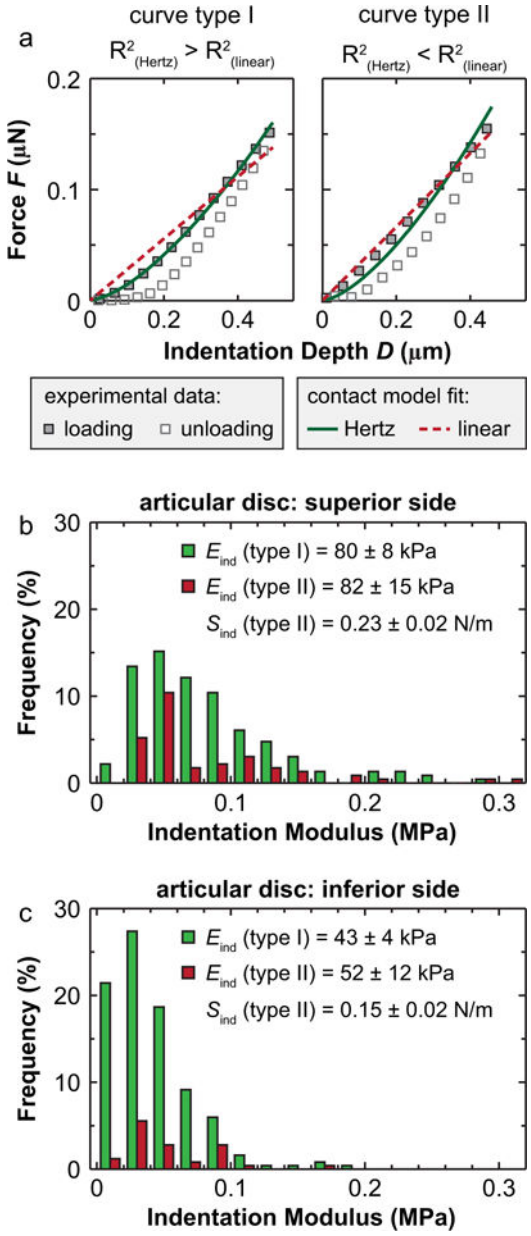

Fig. 8.

Non-Hertzian indentation responses of the TMJ articular disc surface. (a) Two types of representative indentation force versus depth *F-D* curves from the posterior region of the TMJ disc superior surface. Type I: Hertzian indentation curve where $F–D^{3/2}$, where R^2 (Hertz) > R^2 (linear). Type II: linear indentation curve where *F–D*, where R^2 (Hertz) < R^2 (linear). (b, c) Histograms of the distribution of E_{ind} from two indentation curve types on (b) the superior and (c) the inferior surfaces of the TMJ disc (≥300 locations from $n = 7$ animals for each side of the disc measured at 10 μm/s rate. No significant difference in E_{ind} was found between type I and II curves on each surface).